Ultrapermeable Polymers of Intrinsic Microporosity (PIMs) Containing Spirocyclic Units with Fused Triptycenes

C. Grazia Bezzu,* Alessio Fuoco, Elisa Esposito, Marcello Monteleone, Mariagiulia Longo, Johannes Carolus Jansen,* Gary S. Nichol, and Neil B. McKeown*

Polymers of intrinsic microporosity (PIMs), such as the archetypal spirobisindane-based PIM-1, are among the most promising new materials for making gas separation membranes with high permeance for potential use in high-throughput applications. Here it is shown that ultrapermeable PIMs can be prepared by fusing rigid and bulky triptycene (Trip) to the spirobisindane (SBI) unit. PIM-SBI-Trip and its copolymer with PIM-1 (PIM-1/SBI-Trip) are both ultrapermeable after methanol treatment ($P_{CO_2} > 20\,000$ Barrer). Old films, although less permeable, are more selective and therefore provide data that are close to the recently redefined Robeson upper bounds for the important CO_2/CH_4, CO_2/N_2, and O_2/N_2 gas pairs. Temperature-dependent permeation measurements and analysis of the entropic and energetic contributions of the gas transport parameters show that the enhanced performance of these polymers is governed by strong size-sieving character, mainly due to the energetic term of the diffusivity, and related to their high rigidity. Both polymers show a relatively weak pressure-dependence in mixed gas permeability experiments up to 6 bar, suggesting a potential use for CO_2 capture from flue gas or for the upgrading of biogas.

1. Introduction

Gas separation by polymeric membranes is an energy efficient process used to effectively separate industrially and commercially important gas mixtures, such as N_2 or O_2 enrichment

of air, CO_2 from CH_4 for sweetening of natural gas, or H_2 from N_2 for hydrogen recovery during ammonia preparation.[1] In addition, their potential utilisation for the separation of CO_2 from N_2 for post-combustion carbon-capture is being considered, with promising results from pilot-plant scale demonstration studies.[2] For gas separations on such as massive scale, good selectivity and high permeability are required to enhance both the process efficiency and productivity, by reducing the effective size and cost of the membrane system. However, polymeric membranes show a well-known empirical trade-off between permeability (P_a) and selectivity ($\alpha_{ab} = P_a/P_b$) for a given gas pair (a and b), with highly permeable polymers possessing low selectivity and vice versa. The upper bound of this inverse relationship in plots of log P_a versus $\log(P_a/P_b)$, representing the best performing polymeric membranes at the time for the separation of several important gas pairs, was defined for the first time in 1991[3] and then reviewed in 2008 by Robeson.[4] Although these plots are based on single gas permeation data, the position of the gas permeability data for a newly prepared polymeric membrane relative to the 1991 and 2008 upper bounds is used to estimate its potential for gas separations. By a theoretical analysis of the Robeson upper bound, Freeman suggested that its slope results directly from the size-sieving nature of the highly rigid chain of the polymers used to define it, hence increasing both chain rigidity (i.e., diffusivity selectivity) and interchain distance would improve polymer gas permselectivity.[5] Polymers of Intrinsic Microporosity (PIMs) with their contorted and rigid structures, which inhibit efficient packing, adhere closely to this design concept.[6] Indeed, permeability data for PIM-1 (**Figure 1**) and PIM-7 were used to revise the Robeson upper bound for most gas pairs in 2008.[4] Recently, many PIMs with greater chain rigidity have shown improved permeability and selectivity properties with data exceeding the 2008 upper bounds.[7] Their enhanced rigidity was achieved by replacing the relatively flexible spirobisindane (SBI) unit in PIM-1 with spirobifluorene[8] (PIM-SBF-1; Figure 1) or by using stiff bridged bicyclic monomers such as Tröger's base,[9] ethanoanthracene,[9a,10] methanopentacene[11] or triptycene (Trip).[9b,12] In particular, polymers based on the triptycene unit showed remarkable permselectivity so that Pinnau et al.[13] proposed in 2015 to

Dr. C. G. Bezzu, Dr. G. S. Nichol, Prof. N. B. McKeown
EaStCHEM
School of Chemistry
University of Edinburgh
Joseph Black Building, David Brewster Road, Edinburgh
Scotland EH9 3FJ, UK
E-mail: BezzuC@cardiff.ac.uk; Neil.McKeown@ed.ac.uk
Dr. C. G. Bezzu
School of Chemistry
Cardiff University
Main Building, Park Place, Cardiff, Wales CF10 3 AT, UK
Dr. A. Fuoco, Dr. E. Esposito, Dr. M. Monteleone,
M. Longo, Dr. J. C. Jansen
Institute on Membrane Technology
CNR-ITM
Via P. Bucci 17/C, Rende, CS 87036, Italy
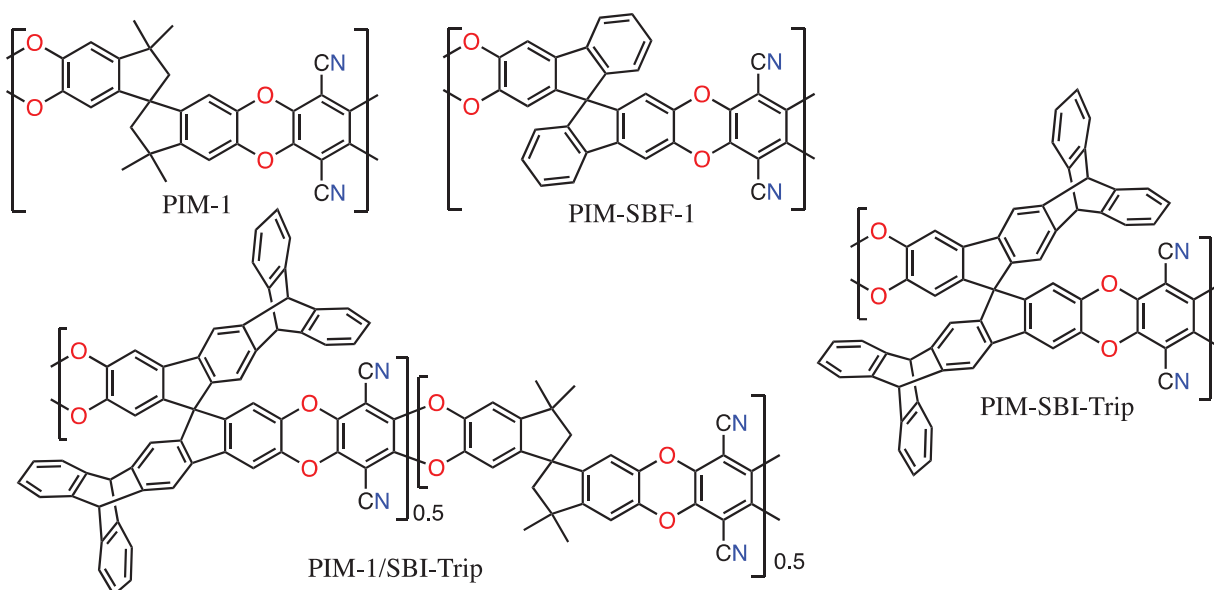E-mail: johannescarolus.jansen@cnr.it

Figure 1. Chemical structures of PIM-1, PIM-SBF-1, and PIM-SBI-Trip along with its copolymer PIM-1/SBI-Trip.

update the O_2/N_2, H_2/N_2, and H_2/CH_4 upper bounds using permeability data from aged films of highly selective triptycene-based PIMs (e.g., PIM-Trip-TB[9b] and TPIM-1[12a]). Recently, we proposed the 2019 revision of the upper bounds for CO_2/N_2 and CO_2/CH_4[14] using data from the ultrapermeable and selective 2D ribbon-shaped benzotriptycene polymers (e.g., PIM-BTrip, PIM-TMN-Trip,[15] and PIM-TFM-BTrip).

Herein we report the synthesis and properties of PIM-SBI-Trip and the copolymer PIM-1/SBI-Trip (Figure 1), derived from a novel structural unit consisting of a spirobisindane to which two rigid and bulky triptycenes have been fused, which was designed to enhance the rigidity of the spirocyclic site of contortion and greatly increase the distance between polymer chains.[16] In addition, we investigate in detail the mechanism of gas transport through the resulting PIMs under a wide range of operating conditions, with pure gases as a function of temperature and with CO_2/N_2 and CO_2/CH_4 gas mixtures as a function of pressure. This allows their potential application in important fields such as carbon capture from flue gas or biogas upgrading to be assessed. In addition, a detailed analysis of the temperature dependence of the permeability and diffusion provides fundamental insight into the energetic and entropic contribution to the high size-selectivity of the membranes.

2. Results and Discussion

2.1. Monomer and Polymer Synthesis

The newly designed monomer, 6,6′,7,7′-(9,10-dihydroanthracene-9,10-diyl)-2,2′,3,3′-tetrahydroxy-9,9′-spiro-bifluorene (SBI-Trip), was prepared by adapting the well-established route to spirobi-fluorenes[17] that is based on the addition of the biphenyl 2-lithio-anion to fluorenone followed by acid-mediated cyclisation (**Figure 2**).

The required triptycene-based 2-bromo-biphenyl precursor (**2**) was prepared by bromination of the corresponding biphenyl (**1**) which was obtained by Suzuki coupling of 3,4-dimethoxyphenylboronic acid with 2-bromotriptycene. Bromo derivative **2** was used to prepare the corresponding fluorenone derivative (**4**) via a one-pot, two-step procedure that involved treatment with *n*-butyl lithium and addition of CO_2 to give the corresponding carboxylic acid (**3**), followed by an acid mediated ring closure (i.e., intramolecular acylation). The lithio-anion derived from **2** was then combined with flu-orenone **4** to give, after acid treatment, the tetramethoxy pre-cursor **5**. Demethylation with boron tribromide afforded the required bis-catechol monomer SBI-Trip **6**. In addition to the
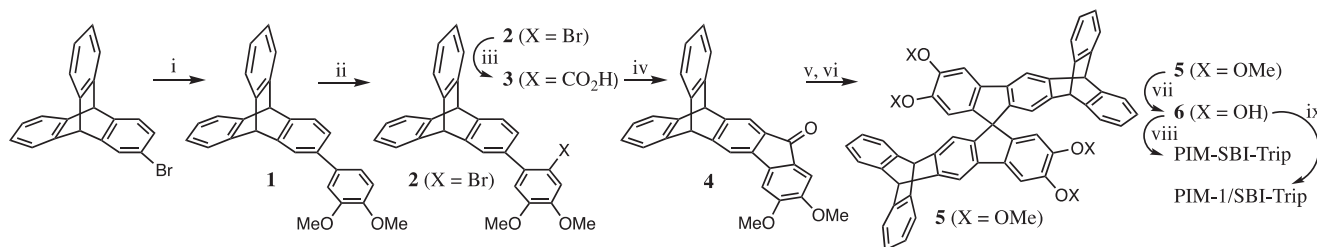
Figure 2. Synthesis of monomer and polymers. Reagent and conditions. i) Pd(PPh₃)₄, K₂CO₃, H₂O/THF, reflux, 24 h; ii) Br₂, CHCl₃, 24 h; iii) *n*-BuLi, CO₂, THF, −78 °C-rt, 3 h; iv) CH₃SO₃H, rt, 3 h; v) 2, *n*-BuLi, THF, −78 °C-rt, 13 h; vi) HCl, CH₃COOH, reflux, 4 h; vii) BBr₃, DCM, 0 °C-rt, 4 h; H₂O; viii) TFTPN, K₂CO₃, DMF, 65 °C, 96 h; ix) TFTPN, SBI, K₂CO₃, DMF, 65 °C, 96 h.
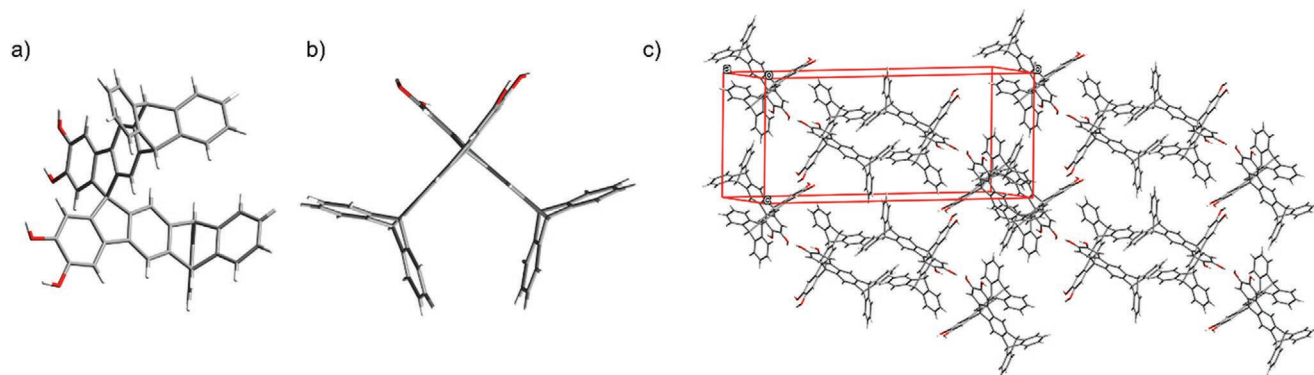
Figure 3. Single crystal XRD structure of monomer SBI-Trip **6**. a) Face-on and b) edge-on molecular view. c) Molecular packing. The included diethyl ether solvent molecules have been removed for clarity. Color code C: grey, O: red, H: white. The unit cell is shown as a red box.

usual spectroscopic methods (e.g., ESI), conformation of the structure of SBI-Trip **6** was obtained by XRD analysis using crystals grown by slow solvent evaporation from a diethyl ether solution. The crystals belong to the monoclinic P2$_1$/c space group with each unit cell containing four SBI-Trip **6** molecules along with sixteen diethyl ether molecules, with which they interact via hydrogen bonding (**Figure 3**). Polymerisation was achieved using the now standard dioxin-forming aromatic nucleophilic substitution reaction between SBI-Trip **6** and 2,3,5,6-tetrafluoroterephthalonitrile (TFTPN). The random copolymer, PIM-1/SBI-Trip, was prepared similarly by reacting an equimolar mixture of SBI-Trip **6** and commercially available 5,5′,6,6″-tetrahydroxy-3,3,3″,3″-tetramethyl-1,1′-spirobisindane (SBI) with TFTPN.

Both polymers proved soluble in chloroform, and were purified by reprecipitation into a non-solvent (acetone and methanol) to remove oligomeric impurities. Analysis by Gel Permeation Chromatography (GPC) of PIM-SBI-Trip and PIM-1/SBI-Trip confirmed their high molecular mass with their weight average molecular mass (M_w) being ≈300×10^3 and 225×10^3 g mol^{-1} relative to polystyrene standards, respectively (**Table 1**). The ESI† gives full experimental details and spectroscopic data for all precursors, monomer and polymers.

Table 1. Properties of PIM-SBI-Trip and PIM-1/SBI-Trip.

Polymer	PIM-SBI-Trip	PIM-1/SBI-Trip
Yield, %	88	85
Solubility	CHCl$_3$	CHCl$_3$
M_w (g mol^{-1})	302 000$^{f)}$	225 000$^{f)}$
M_n/M_w,	2.8	2.1
$SA_{BET}$$^{a)}$ (m^2 g^{-1})	930	858
$V_{Total}$$^{b)}$ (cm^3 g^{-1})	0.72	0.60
$V_M$$^{c)}$, cm^3 g^{-1}	0.33	0.31
CO$_2$ uptake$^{d)}$, (mmol g^{-1})	2.88	2.71
Young's modulus$^{e)}$ (MPa)	2004 (±53)	1790 (±83)

$^{a)}$BET surface area calculated from N$_2$ adsorption isotherm obtained at 77 K; $^{b)}$Total pore volume estimated from N$_2$ uptake at $P/P_0 = 0.98$; $^{c)}$Micropore volume estimated from N$_2$ uptake at $P/P_0 = 0.05$; $^{d)}$CO$_2$ ads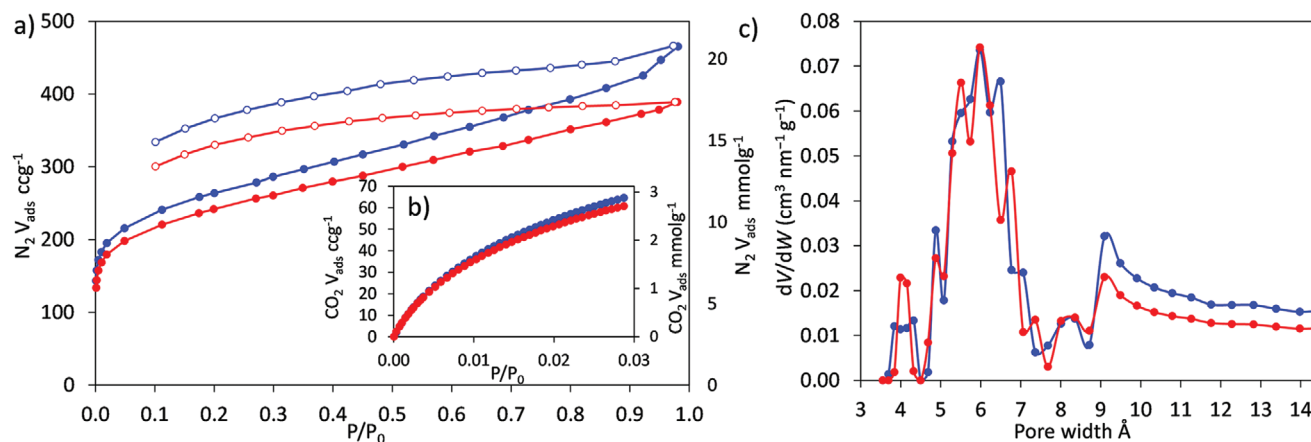orption at 1 bar and 273 K; $^{e)}$Measured by AFM force spectroscopy; $^{f)}$From reprecipitated polymer relative to polystyrene standards.

2.2. Gas Adsorption and Gas Transport Properties

The powdered form of both PIM-SBI-Trip and PIM-1/SBI-Trip adsorbs a significant amount of N$_2$ at low relative pressure ($P/P_0 < 0.05$), at 77 K, indicating significant microporosity. Analysis of the N$_2$ adsorption isotherms (**Figure 4**) provides apparent Brunauer–Emmett–Teller (BET) surface areas (SA$_{BET}$) of 930 and 858 m^2 g^{-1} for PIM-SBI-Trip and PIM-1/SBI-Trip respectively, which are within the upper range for solution processable PIMs,[9a,14,15] and greater than the values reported for PIM-1[18] and PIM-SBF-1.[8] Significantly, PIM-SBI-Trip possesses apparent microporosity that is similar to that of the best performing SBF-based PIMs.[19] This is in agreement with the predictions, based on molecular simulations, that larger substituents on rigid spiro-centre units both frustrate chain packing and increase interchain distances, resulting in enhanced porosity.[20] The shape of the N$_2$ isotherms are similar for both polymers and show a significant gas uptake at higher pressures, followed by a large hysteresis in the desorption isotherms. This can be attributed to the large triptycene substituents reducing cohesion between polymer chains, leading to swelling upon N$_2$ adsorption. Adsorption of CO$_2$ at 273 K (Figure 4b) shows similar uptakes for the two polymers (2.9 and 2.7 mmol g^{-1}, for PIM-SBI-Trip and PIM-1/SBI-Trip, respectively). Micropore size distributions calculated from CO$_2$ adsorption at 273 K using DFT (Figure 4c) are remarkably similar for the two polymers and show a large contribution from ultramicropores (<0.7 nm).

Films were prepared by solution casting, allowing slow solvent evaporation from 3% to 4% w/v polymers solutions in CHCl$_3$ and their Young's moduli were investigated by AFM force spectroscopy measurements (Table 1 and Figure S11: Supporting Information). Sampling scans in different positions of the membrane samples shows a relatively narrow distribution of the Young's modulus in a range of 0.2–0.3 GPa for both polymers (Figure S12, Supporting Information). The averages and standard deviation of the modulus are 2.00 ± 0.05 and 1.79 ± 0.08 GPa for the freshly methanol treated PIM-SBI-Trip and its copolymer, respectively. The modulus of the copolymer PIM-1/SBI-Trip falls between those of the homopolymers PIM-1 and PIM-SBI-Trip. Both polymers are much stiffer than PIM-1[21] but are not as stiff as the very rigid PIM-BTrip,[22] which does not contain spirocyclic units.

Freshly methanol treated self-standing films of PIM-SBI-Trip and PIM-1/SBI-Trip demonstrate ultrapermeability

Figure 4. a) N_2 adsorption (filled symbols) and desorption (open symbols) isotherms at 77 K for PIM-SBI-Trip (●) and PIM-1/SBI-Trip (●). b) CO_2 adsorption and desorption isotherms at 273 K. c) Apparent pore-size distribution (PSD) calculated from CO_2 adsorption data using DFT calculation.
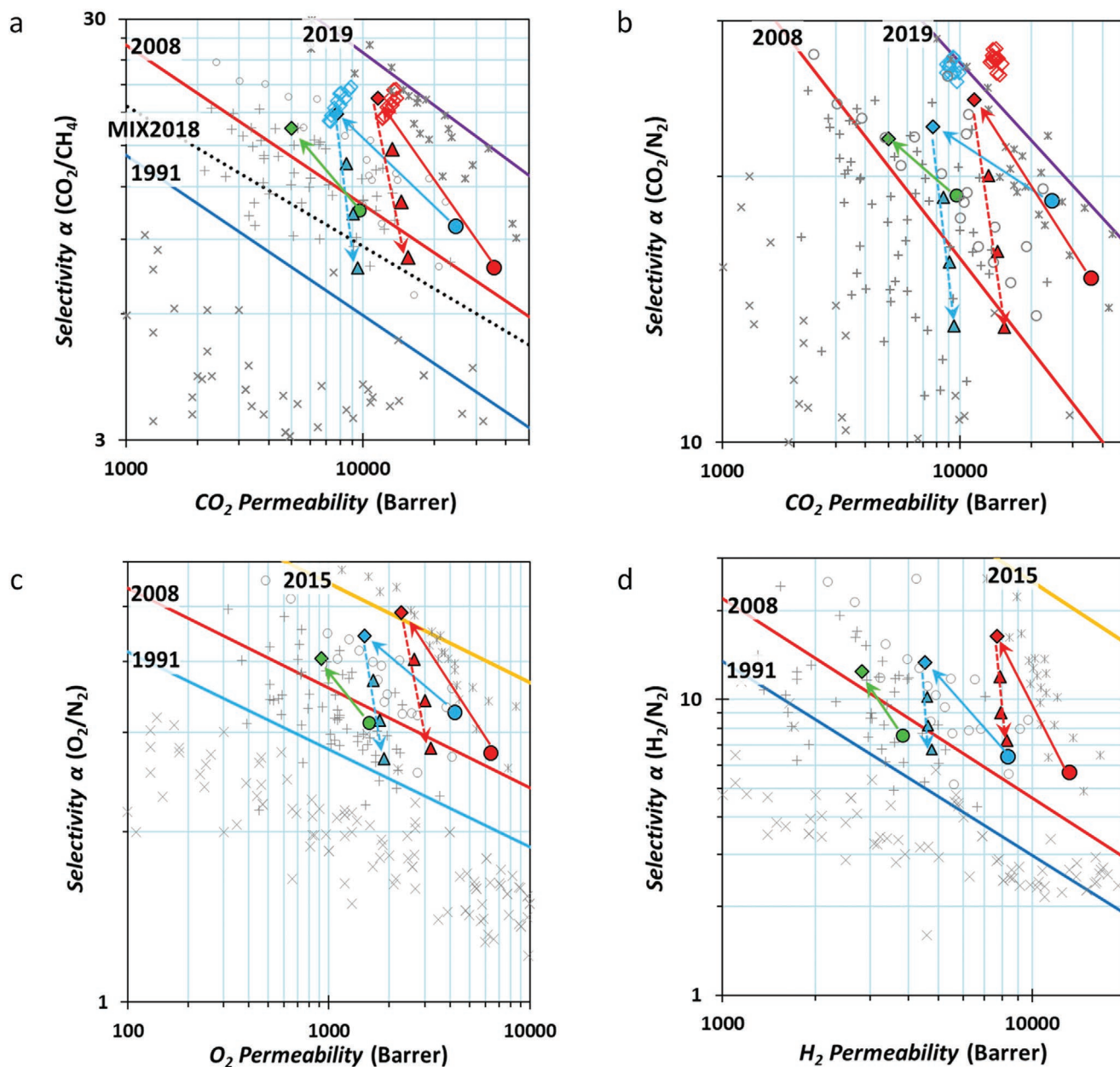
($P_{CO_2} > 20\,000$ Barrer, **Table 2** coupled with moderate selectivities for important gas pairs, with data falling within the same range as that of the 2D benzotriptycene-based PIMs,[14–15] and at much higher selectivities than the archetypal ultrapermeable

polymer poly(trimethylsilylpropyne) (PTMSP). Thus, PIM-SBI-Trip is a unique example of a polymer with chains that are contorted in 3D whose data are located at the ultrapermeable region of the Robeson plots and above the 2008 upper bounds

Table 2. Single gas permeabilities P_a, diffusivity D_a, solubility S_a, and related ideal selectivities α for methanol treated and aged films of PIM-SBI-Trip ($l = 248$ µm) and its copolymer PIM-1/SBI-Trip ($l = 180$ µm), and PIM-1 measured at 25 °C and 1 bar of feed pressure.

Polymer[a]	P_a [Barrer][b]						Ideal selectivity α (P_a/P_b)			
	N_2	O_2	CO_2	CH_4	H_2	He	H_2/N_2	CO_2/N_2	O_2/N_2	CO_2/CH_4
PIM-SBI-Trip[c]	2315	6390	35 600	4600	13 170	4580	5.69	15.4	2.76	7.74
(501 days)[c]	471	2295	11 500	590	7700	2730	16.3	24.4	4.87	19.5
PIM-1/SBI-Trip[c]	1298	4230	24 410	2519	8360	2820	6.44	18.8	3.26	9.69
(401 days)[c]	338	1500	7700	430	4500	1730	13.3	22.8	4.44	17.9
PIM-1[22]	506	1580	9650	913	3830	1560	7.57	19.1	3.12	10.6
(2219 days)[22]	227	917	5000	302	2830	1220	12.5	22.0	4.04	16.6
	D_a [10^{-12} m^2 s^{-1}]						Ideal selectivity α (D_a/D_b)			
	N_2	O_2	CO_2	CH_4	H_2	He	H_2/N_2	CO_2/N_2	O_2/N_2	CO_2/CH_4
PIM-SBI-Trip[c],[d]	273	737	306	115	9340[e]	11 540[e]	34.2	1.12	2.70	2.66
(501 days)[c]	54.3	256	83.8	14.4	5820[e]	9550[e]	107	1.54	4.71	5.82
PIM-1/SBI-Trip[c],[d]	215	734	296	90.6	9490[e]	13 220[e]	44.1	1.38	3.41	3.27
(401 days)[c]	69.5	293	108	21.6	6130[e]	8050[e]	88.2	1.55	4.22	5.00
PIM-1[22]	107	317	131	46.4	5150	5460	48.1	1.22	2.96	2.82
(2219 days)[22]	48.9	188	70.9	16.3	4430	4540	90.6	1.45	3.84	4.35
	S_a [cm^3 cm^{-3} bar^{-1}]						Ideal selectivity α (S_a/S_b)			
	N_2	O_2	CO_2	CH_4	H_2	He	H_2/N_2	CO_2/N_2	O_2/N_2	CO_2/CH_4
PIM-SBI-Trip[c]	6.36	6.50	87.1	29.9	1.06[e]	0.30[e]	0.167	13.7	1.02	2.91
(501 days)[c]	6.51	6.72	103	30.6	0.99[e]	0.21[e]	0.152	15.8	1.03	3.36
PIM-1/SBI-Trip[c]	4.54	4.32	61.9	20.9	0.66[e]	0.16[e]	0.145	13.6	0.95	2.96
(401 days)[c]	3.65	3.84	53.4	14.9	0.55[e]	0.16[e]	0.151	14.6	1.05	3.58
PIM-1[22]	3.55	3.73	55.2	14.8	0.56	0.21	0.16	15.5	1.05	3.73
(2219 days)[22]	3.48	3.65	53.0	13.9	0.48	0.20	0.14	15.2	1.05	3.81

[a]Prior to the permeability measurements, the films were soaked in methanol for 24 h to remove residual solvent, and then dried for 24 h in air. Values between parentheses give the sample age in days of the aged samples; [b]1 Barrer = 10^{-10} cm$^3_{STP}$ cm cm^{-2} s^{-1} cm Hg^{-1}; [c]This work; [d]Associated measured time-lag data are reported in Table S1 (Supporting Information); [e]The calculated values for H_2 and He slightly lose in precision due to the fast membrane time-lag.

**ADVANCED
SCIENCE NEWS**

www.advancedsciencenews.com

**ADVANCED
FUNCTIONAL
MATERIALS**

www.afm-journal.de

Figure 5. Robeson plots for the a) CO_2/CH_4, b) CO_2/N_2, c) O_2/N_2, and d) H_2/N_2 gas pairs with the upper bounds represented by blue lines for 1991,[3] red lines for 2008,[4] yellow lines for 2015 (O_2/N_2 and H_2/N_2),[13] purple lines for 2019[14] (CO_2/N_2 and CO_2/CH_4) and a black dotted line for the upper bound proposed in 2018[24] for the CO_2/CH_4 mixture, at 10 bar CO_2 partial pressure at 35 °C. The gas permeability data for PIM-SBI-Trip are reported in red (freshly MeOH treated (●); and aged 501 days (◆), and in blue for the PIM-1/SBI-Trip co polymer (freshly MeOH treated (●); and aged 401 days (◆). Measurements performed on the aged samples at 35, 45, and 55 °C are reported in triangles (▲▲) with the same color as the corresponding samples tested at 25 °C (◆◆). Data measured in mixed conditions on the aged films are indicated as empty symbols with the borders of the same color (◇,◇). For comparison, the data measured under the same conditions by Longo et al. for PIM-1 after MeOH treatment (●) and 2219 days of ageing (◆) are indicated in green.[22] Other literature data are reported in grey symbols for PIM-1 (+), SBF-based PIMs (○), ultrapermeable triptycene based PIMs (✳) and PTMSP (×).

(**Figure 5**). The order of gas permeability is $CO_2 > H_2 > O_2 > He \approx CH_4 > N_2$, and the similar values for He and CH_4 show that the permeability is strongly influenced by both the diffusion and the sorption coefficients. The high CH_4 permeability is due to its remarkably high solubility coefficient, which is among the highest known for any polymer (Table 2).[9a,14,15] The PIM-1/SBI-Trip 1:1 copolymer demonstrates gas permeability data that lie

neatly between those of the two parent homo polymers PIM-SBI-Trip and PIM-1 (Figure 5). The very high gas permeabilities of these two PIMs measured from freshly methanol treated films decrease over time (Table 2) due to physical ageing, a well-known feature of all high free volume glassy polymers.[23] The decrease in permeability is mainly due to lower diffusion coefficients (**Figure 6** and Figure S13a: Supporting Information),

**ADVANCED
SCIENCE NEWS**

www.advancedsciencenews.com

**ADVANCED
FUNCTIONAL
MATERIALS**

www.afm-journal.de

Figure 6. Relative changes of the diffusion coefficients of He/N$_2$ and CO$_2$/N$_2$ for PIM-SBI-Trip are reported in red (freshly MeOH treated (●); and aged 501 days (◆), and in blue for the PIM-1/SBI-Trip copolymer (freshly MeOH treated (●); and aged 401 days (◆). Measurements performed on the aged samples at 35, 45 and 55 °C are reported in triangles (▲▲) with the same color as the corresponding samples tested at 25 °C (◆◆). The solid line represents the fitted average data of glassy polymers reported by Robeson et al.[25]

while solubility is not as significantly influenced by ageing (Figure S13b, Supporting Information).

The decrease in permeability is combined with a strong increase in selectivity, which places the data of aged PIM-SBI-Trip on the 2015 upper bound for O$_2$/N$_2$, with similar selectivity to that of commercial polymers used to produce membranes but with two-orders of magnitude higher permeability, and close to the 2019 upper bounds for CO$_2$/CH$_4$ and CO$_2$/N$_2$ gas pairs (Figure 5). For the H$_2$/N$_2$ gas pair, the trend upon ageing is also much steeper than the Robeson upper bound. The decrease in permeability is connected to the loss of larger elements of free volume over time resulting in a greater degree of ultramicroporosity and enhanced size-selectivity. The effect on permeability is stronger for bulkier gases with respect to smaller ones, for example, after 500 days of ageing, CH$_4$ loses 88% of its diffusion coefficient while He decreases only 17%, resulting in a marked increase in He/CH$_4$ permselectivity. This is clearly illustrated by the steeper correlation between the effective gas diameter, d_{eff}^2, and the diffusion coefficient, D (Figure S13a, Supporting Information).

Additional measurements on the aged films of PIM-SBI-Trip and PIM-1/SBI-Trip were carried out at temperatures of 25, 35, 45, and 55 °C (Figure 5 and Figure S14: Supporting Information). The gas diffusion coefficients increase with temperature (Figure S15, Supporting Information) with the aged membrane demonstrating very similar diffusivities as the freshly MeOH treated membrane at 25 °C (Figure 6).

Permeabilities (Figure S14, Supporting Information) also increase as a function of temperature due to the increasing

diffusion coefficients, but they are not fully restored (Figure 5) since solubility decreases (Figure S16, Supporting Information). At higher temperature, the selectivities for all gas pairs decrease so that at 55 °C they are roughly similar to those of the freshly methanol treated samples at 25 °C.

The trends of P, D, and S as a function of temperature follow Arrhenius behavior described by Equations (1–3)

$$P = P_0 \exp\left(\frac{-E_p}{RT}\right) \tag{1}$$

$$D = D_0 \exp\left(\frac{-E_d}{RT}\right) \tag{2}$$

$$S = S_0 \exp\left(\frac{-H_s}{RT}\right) \tag{3}$$

Where, R is the universal gas constant; T the absolute temperature; P_0, D_0, and S_0 are the pre-exponential factors and define the intercept on the vertical axis in the Arrhenius plot, E_p is the activation energy of permeation, E_d the activation energy of diffusion, and H_s the heat of sorption. For both PIM-SBI-Trip and in PIM-1/SBI-Trip, E_p is higher than that of the triptycene-based ultrapermeable PIMs.[26] Both polymers show among the highest values of H_s reported for PIMs (**Table 3**), indicating a strong polymer-sorbent interaction and high sorption capability. The large values of E_d for larger gases (i.e., N$_2$ and CH$_4$) correlate to the strong size-sieving properties of the polymers that result in their high diffusion selectivity (Table 2). Although there are some differences in the like-to-like comparison between specific gas pairs, the two polymers have comparable size-sieving properties, as highlighted by the similar slope of the activation energy of diffusion as a function of the square effective diameter of the penetrant gases (Figure S17, Supporting Information). According to the transition theory of diffusion,[27] the diffusion selectivity between two gases a and b (D_a/D_b) can be defined as:

$$\frac{D_a}{D_b} = \frac{\lambda_a^2}{\lambda_b^2} \underbrace{\exp\left(\frac{\Delta S_{d(a,b)}}{R}\right)}_{\text{entropic selectivity}} \underbrace{\exp\left(-\frac{\Delta E_{d(a,b)}}{RT}\right)}_{\text{energetic selectivity}} \tag{4}$$

where λ_a and λ_b are the average diffusive jumps for gas a and b; $\Delta S_{d(a,b)}$ is the difference in the activation entropy of diffusion, i.e., $\Delta S_{d(a,b)} = (S_{d,a}^* - S_{d,a}) - (S_{d,b}^* - S_{d,b})$ where S_d^* and S_d are the entropies of the gas a and b in the activated (in the transition region) and normal (in the micropores) states respectively,[28] and it defines the entropic selectivity; and $\Delta E_{d(a,b)}$ is the difference in the activation energies of diffusion, which influences the energetic selectivity. λ_a and λ_b are generally unknown for a specific matrix, but the ratio λ_a^2/λ_b^2 can be approximated as d_a^2/d_b^2, where d is the effective diameter of the penetrant gas,[29] allowing the estimation of the entropic and energetic contributions. The entropic selectivity is related to the changes in the degree of freedom of one gas during its diffusion process from the micropores (normal state) to the motion-enabled zone (transition state), and it is a characteristic of molecular sieve materials. The entropic selectivity is below 1 for O$_2$/N$_2$, CO$_2$/N$_2$, H$_2$/N$_2$, and He/N$_2$, which means that in the normal state

Table 3. Activation energies for permeation (E_p) and diffusion (E_d), heat of sorption (H_s), diffusion selectivity (D_a/D_{N_2}) for gas transport and correlated energetic and entropic selectivity with respect to N_2 at 25 °C in aged films of PIM-SBI-Trip and the copolymer PIM-1/SBI-Trip as compared to the values for the archetypal PIM-1.

Property	Polymer	Gas					
		N_2	O_2	CO_2	CH_4	H_2	He
E_p [kcal mol^{-1}]	PIM-SBI-Trip[a],[b]	5.79 ± 0.18	2.23 ± 0.21	1.91 ± 0.21	7.61 ± 0.04	0.44 ± 0.12	1.08 ± 0.31
	PIM-1/SBI-Trip[a],[b]	4.74 ± 0.17	1.47 ± 0.13	1.36 ± 0.15	6.88 ± 0.06	0.33 ± 0.06	0.65 ± 0.06
	PIM-1[30]	2.8	0.6	0.4	4.2	0.4	0.6
H_s [kcal mol^{-1}]	PIM-SBI-Trip[a],[b]	−3.92 ± 0.01	−3.60 ± 0.66	−5.32 ± 0.09	−4.71 ± 0.06	−1.93 ± 0.32[c]	−1.02 ± 1.65[c]
	PIM-1/SBI-Trip[a],[b]	−3.86 ± 0.09	−4.03 ± 0.10	−5.03 ± 0.12	−3.96 ± 0.04	−1.47 ± 0.29[c]	−1.32 ± 1.13[c]
	PIM-1[30]	−3.1	−4.7	−3.8	−3.7	−2.8	−2.4
E_d [kcal mol^{-1}]	PIM-SBI-Trip[a],[b]	9.71 ± 0.18	5.83 ± 0.51	7.23 ± 0.11	12.33 ± 0.08	2.37 ± 0.30[c]	2.10 ± 1.45[c]
	PIM-1/SBI-Trip[a],[b]	8.60 ± 0.10	5.50 ± 0.04	6.40 ± 0.06	10.84 ± 0.09	1.80 ± 0.23[c]	1.98 ± 1.09[c]
	PIM-1[30]	6	5.3	4.2	7.8	3.2	3
Diffusion selectivity D_a/D_{N_2}	PIM-SBI-Trip[a]	–	4.72	1.54	0.266	107[c]	176[c]
	PIM-1/SBI-Trip[a]	–	4.22	1.56	0.31	88.2[c]	116[c]
	PIM-1[26]	–	2.93	1.60	0.33	45.3	44.0
Energetic selectivity (see Equation (4))	PIM-SBI-Trip[a],[b]	–	716 ± 127	66.8 ± 7.9	0.012 ± 0.001	$2.45 \cdot 10^5 ± 0.15 \ 10^{5}$[c]	$3.88 \cdot 10^5 ± 0.82 \ 10^{5}$[c]
	PIM-1/SBI-Trip[a],[b]	–	188 ± 8.5	41.4 ± 3.1	0.023 ± 0.002	$9.79 \cdot 10^4 ± 0.48 \ 10^{4}$[c]	$7.26 \cdot 10^4 ± 1.29 \ 10^{4}$[c]
	PIM-1[26]	–	3.26	20.9	0.048	113	159
Entropic selectivity (see Equation (4))	PIM-SBI-Trip[a],[b]	–	0.007 ± 0.001	0.024 ± 0.003	20.17 ± 2.00	$0.9 \cdot 10^{-3} ± 0.6 \cdot 10^{-4}$[c]	$1.3 \cdot 10^{-3} ± 2.9 \cdot 10^{-4}$[c]
	PIM-1/SBI-Trip[a],[b]	–	0.025 ± 0.001	0.038 ± 0.003	12.4 ± 1.0	$1.8 \cdot 10^{-3} ± 0.9 \cdot 10^{-4}$[c]	$4.7 \cdot 10^{-3} ± 8.3 \cdot 10^{-4}$[c]
	PIM-1[26]	–	0.99	0.077	6.37	0.81	0.81

[a]This work; [b]Experimental errors associated to these data are calculated via linear regression of the diffusion coefficients as a function of the temperature and via the error propagation theory; [c]The calculated values for H_2 and He may slightly lose in precision due to the fast membrane time-lag.

(i.e., during the diffusion within a micropore) the smaller gas has more translational freedom, while in the transition state (i.e., diffusion between two micropores), all degrees of freedom are suppressed. For a similar reason, the entropic selectivity for CH_4/N_2 is above 1, since N_2 is the smallest of the two gas molecules. Even, if at a first glance, a diffusion selectivity term that favors the selectivity of bigger molecules over the smaller ones is counter-intuitive, it is based on thermodynamic laws, since smaller molecules have more translational and rotational freedom on their molecular axes in the permanent microporosity of PIMs with respect to bigger molecules, and both have zero freedom in the transition region. This means that smaller molecules lose more entropy, which is a less favored thermodynamic process. The high value for CH_4/N_2 entropic selectivity, and low values for the other gas pairs, indicate the presence of larger voids in the polymer microstructure of PIM-SBI-Trip as compared to other ultrapermeable PIMs such as PIM-TMN-Trip and PIM-BTrip. The energetic selectivity is proportional to the energy required to open motion-enabled-regions to allow the transport of one relative to another, and it is the governing factor of the diffusion separation in polymers discussed previously.[26–28]

This is the main factor that governs the size-sieving character of PIM-SBI-Trip and PIM-1/SBI-Trip and both polymers show values that are among the highest reported for PIMs (Table 3). This

is ascribed to the overall rigidity of these polymers (Figure S12, Supporting Information), provided by the phenyl ring of the fused triptycene units reducing the flexibility about the spiro-centre, as found for the spirobisfluorene PIMs (e.g., PIM-SBF-1),[8,19] and the inherent rigidity provided by these bridged bicyclic substituents. He and H_2 have high energetic selectivity when related to N_2 since their diffusion requires only small thermal motions of the polymer chains. Remarkably, the energetic selectivity for O_2/N_2 in PIM-SBI-Trip is about 9 times higher than the best performing semi-rigid polymer 6FDA/PMDA(10/90)-TAB,[28] and that of the ultrapermeable PIM-BTrip.[26] PIM-BTrip and PIM-SBI-Trip have similar BET surface areas, i.e., 911 and 930 m^2 g^{-1} respectively. As the overall rigidities of these two PIMs are expected to be similar, the higher energetic selectivity of PIM-SBI-Trip may be related to packing of its 3D contorted chains resulting in a higher proportion of smaller micropores relative to that of the 2D chains of PIM-BTrip.

2.3. Mixed Gas Permeation

Gas mixtures of CO_2/CH_4 (35/65 vol%, **Figure 7**a,b), simulating biogas, and CO_2/N_2 (15/85 vol%, Figure 7c,d), simulating typical flue gas, were used to assess the performance of the PIM-SBI-Trip and PIM-1/SBI-Trip membranes, according to
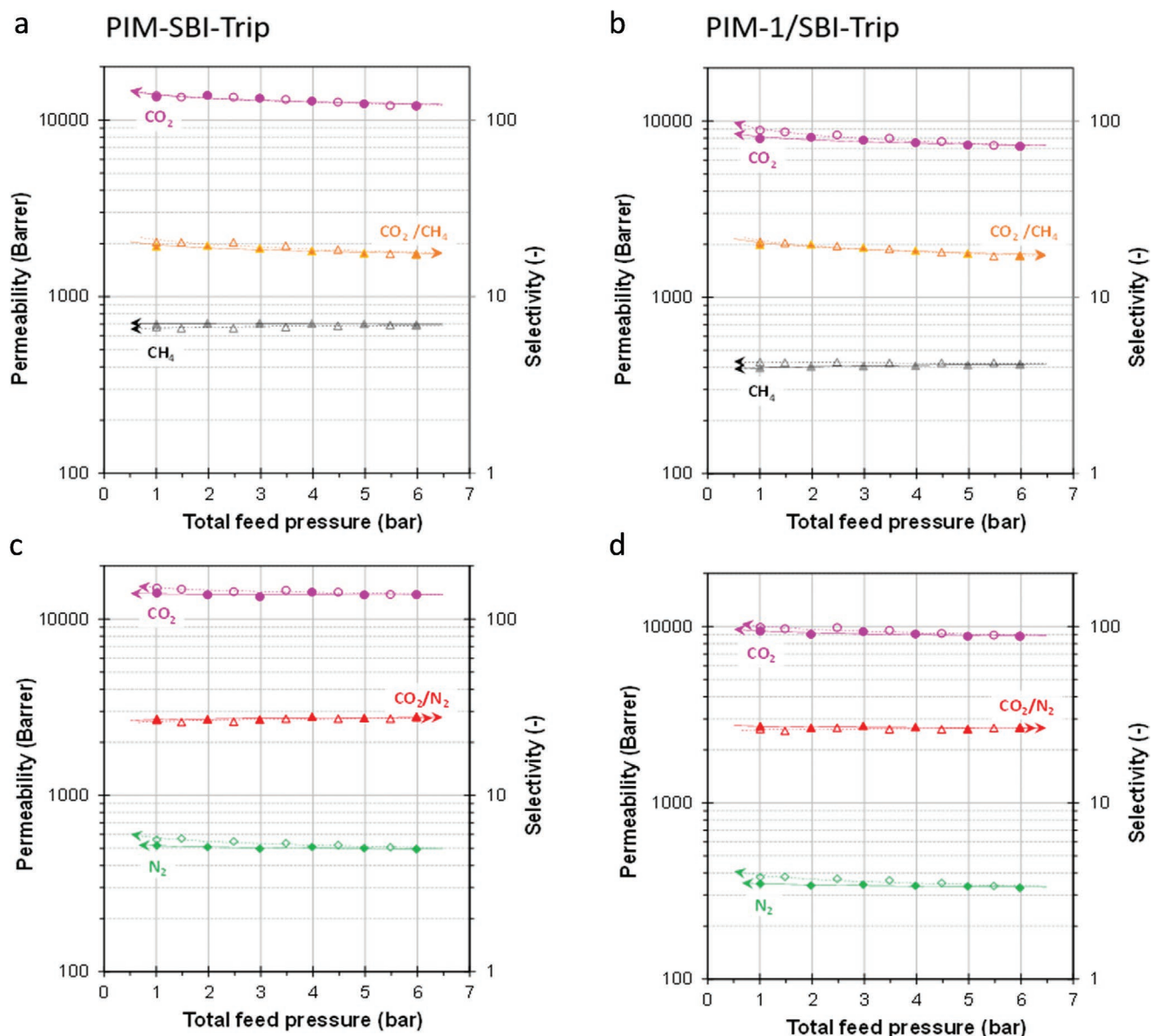
Figure 7. a,c) Mixed gas permeation in the aged films of PIM-SBI-Trip and in its copolymer b,d) PIM-1/SBI-Trip as a function of the total feed pressure. Mixture CO_2/CH_4 (35/65 vol%) simulating biogas (a,b), and Mixture CO_2/N_2 (15/85 vol%) simulating a typical flue gas composition (c,d). Closed symbols and full lines represent the stepwise increasing pressure; open symbols and dashed lines represent the subsequent stepwise decreasing pressure. Lines are plotted as a guide to the eye and the arrows indicate the axis where to read the data. The analogous figures as a function of the CO_2 partial pressure are given in Figure S19 (Supporting Information).

a previously reported procedure.[31] Ultrapermeable polymers easily lead to a high stage-cut, where the separation factor depends on the process conditions as much as the material properties.[32] The experiments in this work were therefore carried out at low stage-cut (≪1%, see Figure S18, Supporting Information), using a small membrane area, a high feed flow rate and a relatively high sweep flow rate, in order to focus mainly on the materials properties. The gas permeability in both PIM-SBI-Trip-based films shows a modest feed pressure dependence, similarly to that prepared from PIM-SBF-1.[33] CO_2 permeability decreases with increasing feed pressure due to the saturation of Langmuir sites, which is a typical feature for

materials showing dual mode sorption without undergoing strong swelling and/or plasticization. There is only weak hysteresis between mixed gas permeability measurements at increasing and then decreasing pressures in PIM-1/SBI-Trip. The slightly higher permeability during the pressure-decrease steps indicates a weak dilation of the polymer matrix at a higher partial pressure of CO_2 in the feed at higher total pressures or in CO_2 rich mixtures (Figure 7b). For both PIM-SBI-Trip and PIM-1/SBI-Trip, the mixed gas permeability data for the CO_2/CH_4 gas pair at 1–6 bar are similar to that obtained from single gas measurements and close to the 2019[14] upper bound. Although obtained at lower partial pressure, these data are also

**ADVANCED
SCIENCE NEWS**

www.advancedsciencenews.com

**ADVANCED
FUNCTIONAL
MATERIALS**

www.afm-journal.de

well above the proposed 2018 CO_2/CH_4 upper bound for mixed gases at a CO_2 partial pressure of 10 bar[24] (Figure 5a).

For both polymers, the CO_2/N_2 mixed gas permeability data lie in a more favorable position of the Robeson plot as compared to the single gas data (Figure 4b), and for PIM-SBI-Trip they are even above the 2019 upper bound. Remarkably, the mixed gas performance of PIM-SBI-Trip and PIM-1/SBI-Trip shows systematically higher selectivities than aged PIM-TMN-Trip and with similar CO_2 permeability (Figure S20, Supporting Information), demonstrating the potential of these ultrapermeable PIMs for biogas upgrading[32] and CO_2 capture from flue gases.[34] Previous work with benchmark polymer PIM-1 shows significantly improved selectivity in hollow fiber membranes,[35] suggesting that also for the present polymers even better separation performance may be expected when prepared in the form of asymmetric or thin film composite membranes.

3. Conclusion

Fusing two bulky and rigid triptycene units to the SBI site of contortion provides a PIM with increased intrinsic microporosity, as demonstrated by enhanced gas adsorption and permeability. The resulting PIM-SBI-Trip and PIM-1/SBI-Trip are the first ultrapermeable PIMs in which the polymer chains are contorted in 3D. Their excellent permselectivity data, in particular for the CO_2/CH_4 and CO_2/N_2 gas pairs, and the modest pressure dependence in mixed gas conditions, albeit demonstrated only at relatively low pressures, make these particularly promising materials for CO_2-related separations. In addition, PIM-SBI-Trip shows similar selectivity as traditional polymers used in industrial O_2/N_2 separation, but at much higher permeability, paving the way to the development of compact O_2 production or enrichment systems. This may be relevant to the development of small-scale oxygen generators for medical use in home or hospital by patients with respiratory diseases.

Supporting Information

Supporting Information is available from the Wiley Online Library or from the author.

Conflict of Interest

The authors declare no conflict of interest.

Data Availability Statement

The data that supports the findings of this study are available in the supplementary material of this article.

[1] a) R. S. Murali, T. Sankarshana, S. Sridhar, *Sep. Purif. Rev.* **2013**, *42*, 130; b) S. Wang, X. Li, H. Wu, Z. Tian, Q. Xin, G. He, D. Peng, S. Chen, Y. Yin, Z. Jiang, *Energy Environ. Sci.* **2016**, *9*, 1863; c) C. A. Scholes, G. W. Stevens, S. E. Kentish, *Fuel* **2012**, *96*, 15; d) J. Adewole, A. Ahmad, *J. Polym. Res.* **2017**, *24*, 70; e) E. Esposito, L. Dellamuzia, U. Moretti, A. Fuoco, L. Giorno, J. C. Jansen, *Energy Environ. Sci.* **2019**, *12*, 281; f) P. Bernardo, E. Drioli, G. Golemme, *Ind. Eng. Chem. Res.* **2009**, *48*, 4638; g) Y. Yampolskii, *Macromolecules* **2012**, *45*, 3298; h) E. Lasseuguette, M.-C. Ferrari, in *Sustainable Nanoscale Engineering*, Elsevier, New York **2020**, p. 265; i) A. Iulianelli, E. Drioli, *Fuel Process. Technol.* **2020**, *206*, 106464; j) R. W. Baker, B. T. Low, *Macromolecules* **2014**, *47*, 6999.

[2] L. S. White, K. D. Amo, T. Wu, T. C. Merkel, *J. Membr. Sci.* **2017**, *542*, 217.

[3] L. M. Robeson, *J. Membr. Sci.* **1991**, *62*, 165.

[4] L. M. Robeson, *J. Membr. Sci.* **2008**, *320*, 390.

[5] a) L. Robeson, B. Freeman, D. Paul, B. Rowe, *J. Membr. Sci.* **2009**, *341*, 178; b) B. D. Freeman, *Macromolecules* **1999**, *32*, 375.

[6] a) P. M. Budd, E. S. Elabas, B. S. Ghanem, S. Makhseed, N. B. McKeown, K. J. Msayib, C. E. Tattershall, D. Wang, *Adv. Mater.* **2004**, *16*, 456; b) M. Heuchel, D. Fritsch, P. M. Budd, N. B. McKeown, D. Hofmann, *J. Membr. Sci.* **2008**, *318*, 84.

[7] M. D. Guiver, Y. M. Lee, *Science* **2013**, *339*, 284.

[8] C. G. Bezzu, M. Carta, A. Tonkins, J. C. Jansen, P. Bernardo, F. Bazzarelli, N. B. McKeown, *Adv. Mater.* **2012**, *24*, 5930.

[9] a) M. Carta, R. Malpass-Evans, M. Croad, Y. Rogan, J. C. Jansen, P. Bernardo, F. Bazzarelli, N. B. McKeown, *Science* **2013**, *339*, 303; b) M. Carta, M. Croad, R. Malpass-Evans, J. C. Jansen, P. Bernardo, G. Clarizia, K. Friess, M. Lanč, N. B. McKeown, *Adv. Mater.* **2014**, *26*, 3526.

[10] a) Y. Rogan, L. Starannikova, V. Ryzhikh, Y. Yampolskii, P. Bernardo, F. Bazzarelli, J. C. Jansen, N. B. McKeown, *Polym. Chem.* **2013**, *4*, 3813; b) E. Tocci, L. De Lorenzo, P. Bernardo, G. Clarizia, F. Bazzarelli, N. B. Mckeown, M. Carta, R. Malpass-Evans, K. Friess, K. t. Pilnáček, *Macromolecules* **2014**, *47*, 7900; c) X. Ma, I. Pinnau, *Macromolecules* **2018**, *51*, 1069.

[11] R. Williams, L. A. Burt, E. Esposito, J. C. Jansen, E. Tocci, C. Rizzuto, M. Lanč, M. Carta, N. B. McKeown, *J. Mater. Chem. A* **2018**, *6*, 5661.

[12] a) B. S. Ghanem, R. Swaidan, X. Ma, E. Litwiller, I. Pinnau, *Adv. Mater.* **2014**, *26*, 6696; b) B. S. Ghanem, R. Swaidan, E. Litwiller, I. Pinnau, *Adv. Mater.* **2014**, *26*, 3688; c) I. Rose, M. Carta, R. Malpass-Evans, M.-C. Ferrari, P. Bernardo, G. Clarizia, J. C. Jansen, N. B. McKeown, *ACS Macro Lett.* **2015**, *4*, 912.

[13] R. Swaidan, B. Ghanem, I. Pinnau, *ACS Macro Lett.* **2015**, *4*, 947.

[14] B. Comesaña-Gándara, J. Chen, C. G. Bezzu, M. Carta, I. Rose, M.-C. Ferrari, E. Esposito, A. Fuoco, J. C. Jansen, N. B. McKeown, *Energy Environ. Sci.* **2019**, *12*, 2733.

[15] I. Rose, C. G. Bezzu, M. Carta, B. Comesaña-Gándara, E. Lasseuguette, M. C. C. Ferrari, P. Bernardo, G. Clarizia, A. Fuoco, J. C. Jansen, K. E. E. Hart, T. P. Liyana-Arachchi, C. M. Colina, N. B. McKeown, *Nat. Mater.* **2017**, *16*, 932.

[16] T. M. Long, T. M. Swager, *Adv. Mater.* **2001**, *13*, 601.

[17] R. G. Clarkson, M. Gomberg, *J. Am. Chem. Soc.* **1930**, *52*, 2881.

[18] P. M. Budd, B. S. Ghanem, S. Makhseed, N. B. McKeown, K. J. Msayib, C. E. Tattershall, *Chem. Commun.* **2004**, 230.

**ADVANCED
SCIENCE NEWS**

www.advancedsciencenews.com

**ADVANCED
FUNCTIONAL
MATERIALS**

www.afm-journal.de

[19] C. G. Bezzu, M. Carta, M.-C. Ferrari, J. C. Jansen, M. Monteleone, E. Esposito, A. Fuoco, K. Hart, T. P. Liyana-Arachchi, C. M. Colina, N. B. McKeown, *J. Mater. Chem. A* **2018**, *6*, 10507.

[20] K. E. Hart, J. M. Springmeier, N. B. McKeown, C. M. Colina, *Phys. Chem. Chem. Phys.* **2013**, *15*, 20161.

[21] a) Q. Song, S. Cao, R. H. Pritchard, B. Ghalei, S. A. Al-Muhtaseb, E. M. Terentjev, A. K. Cheetham, E. Sivaniah, *Nat. Commun.* **2014**, *5*, 4813; b) K. Polak-Kraśna, C. Fuhrhop, S. Rochat, A. D. Burrows, A. Georgiadis, C. R. Bowen, T. J. Mays, *Int. J. Hydrogen Energy* **2017**, *42*, 23915; c) K. Polak-Kraśna, R. Dawson, L. T. Holyfield, C. R. Bowen, A. D. Burrows, T. J. Mays, *J. Mater. Sci.* **2017**, *52*, 3862.

[22] M. Longo, M. P. De Santo, E. Esposito, A. Fuoco, M. Monteleone, L. Giorno, B. Comesaña-Gándara, J. Chen, C. G. Bezzu, M. Carta, I. Rose, N. B. McKeown, J. C. Jansen, *Ind. Eng. Chem. Res.* **2020**, *59*, 5381.

[23] Z.-X. Low, P. M. Budd, N. B. McKeown, D. A. Patterson, *Chem. Rev.* **2018**, *118*, 5871.

[24] Y. Wang, X. Ma, B. S. Ghanem, F. Alghunaimi, I. Pinnau, Y. Han, *Mater. Today Nano* **2018**, *3*, 69.

[25] L. M. Robeson, Z. P. Smith, B. D. Freeman, D. R. Paul, *J. Membr. Sci.* **2014**, *453*, 71.

[26] A. Fuoco, B. Comesaña-Gándara, M. Longo, E. Esposito, M. Monteleone, I. Rose, C. G. Bezzu, M. Carta, N. B. McKeown, J. C. Jansen, *ACS Appl. Mater. Interfaces* **2018**, *10*, 36475.

[27] W. J. Koros, C. Zhang, *Nat. Mater.* **2017**, *16*, 289.

[28] C. M. Zimmerman, W. J. Koros, *Macromolecules* **1999**, *32*, 3341.

[29] a) J. Crank, *The Mathematics of Diffusion*, Clarendon Press, Oxford **1975**; b) A. Singh-Ghosal, W. J. Koros, *Ind. Eng. Chem. Res.* **1999**, *38*, 3647.

[30] P. Li, T. Chung, D. Paul, *J. Membr. Sci.* **2014**, *450*, 380.

[31] S. C. Fraga, M. Monteleone, M. Lanč, E. Esposito, A. Fuoco, L. Giorno, K. Pilnáček, K. Friess, M. Carta, N. B. McKeown, P. Izák, Z. Petrusová, J. G. Crespo, C. Brazinha, J. C. Jansen, *J. Membr. Sci.* **2018**, *561*, 39.

[32] P. Stanovsky, M. Karaszova, Z. Petrusova, M. Monteleone, J. C. Jansen, B. Comesaña-Gándara, N. B. McKeown, P. Izak, *J. Membr. Sci.* **2021**, *618*, 118694.

[33] M. Monteleone, E. Esposito, A. Fuoco, M. Lanč, K. Pilnáček, K. Friess, C. G. Bezzu, M. Carta, N. B. McKeown, J. C. Jansen, *Membranes* **2018**, *8*, 73.

[34] P. Stanovsky, A. Zitkova, M. Karaszova, M. Šyc, J. C. Jansen, B. C. Gándara, N. B. McKeown, P. Izak, *Sep. Purif. Technol.* **2020**, *242*, 116814.

[35] M. L. Jue, V. Breedveld, R. P. Lively, *J. Membr. Sci.* **2017**, *530*, 33.